Synthesis and Investigation of V-shaped Hole-Transporting Materials Containing Tröger`s Base Core and TPD-type Branches

Titas Braukyla, † [a] Nobuya Sakai, † [b] Maryte Daskeviciene,[a] Vygintas Jankauskas,[c] Egidijus Kamarauskas,[c] Tadas Malinauskas,[a] Regimantas Komskis [d], Saulius Jursenas [d], Henry J. Snaith,*[b] Vytautas Getautis*[a]

Abstract: Novel V-shaped hole transporting materials based on TPD-type moieties conjoined by a Tröger`s base core were synthesized and investigated. These hole transporting materials (HTMs) obtained by synthetic method of merely three steps are fully amorphous and possess high glass transition temperatures, good thermal and morphological stability, are easily processable and have comparatively high charge mobility (up to 0.036 $cm^2 V^{-1} s^{-1}$). Measured ionization potentials are not exceeding value of perovskite for methylammonium lead iodide ($CH_3NH_3PbI_3$). These observations are suggesting that synthesized compounds are compatible with and can be used in fabrication of perovskite solar cells.

Introduction

Technological progress and growing human population consequently upsurge energy demand and forces to seek alternatives for conventional sources such as non-replenishing fossil fuel deposits. Solar power seems to be a desired option as it is the primal and direct source from which majority of other renewable energy sources originate. Harnessing the power of light and transforming it into electricity as a form more suitable for transfer, accumulation and usage can be directly achieved by solar cells. Even though solar cell technology and production from inorganic materials, mainly crystalline silica which currently occupies about 90 percent of photovoltaic market,[1] is already well developed it also faces problems deriving from their compositional materials themselves – alternatively, organic and hybrid solar cells overcome those drawbacks as these cells are inexpensive, light, flexible, requires less energy to produce and consists of abundant chemical elements.[2] Among these solar cells perovskite layer containing ones seem certainly promising as their relatively new yet constantly evolving technology already allowed to reach power conversion efficiency (PCE) of 22.1 percent in single-junction perovskite solar cell.[3]

Efficiency of perovskite solar cell (PSC) highly depends on HTM which is expected to have good hole-drift mobility and high morphological stability as well as to meet certain HOMO and LUMO energy requirements. 2,2′,7,7′-tetrakis(4,4′-dimethoxydiphenylamino)-9,9′-spirobifluorene (spiro-OMeTAD) is the most widely used small-molecule class HTM in both solid-state dye-sensitized solar cells (ssDSSCs)[4][5] and PSCs.[6-10] Even though Spiro-MeOTAD is unrivaled efficiency wise by its counterparts in PSC the compound itself also have its flaws. Spiro-OMeTAD is found to exist in semicrystalline state and has a tendency to crystallize in the device, thus impairing cell's performance[11]. Crystallization of the hole conductor layer is undesirable for it would impair the formation of a good contact among the active layer and back contact electrodes.[12] Such findings encourage a search for novel HTM alternatives.

Linkage between Spiro-MeOTAD structural features and its high efficiency as HTM is of significant importance. It is considered that spiro-OMeTAD (Fig. 1a) is conceptually derived mostly from the respective TPD-type compounds conjoined by spiro center orientating TPDs perpendicularly to one another.[13] Also a study of Nukada, Sato and Akasaki shows how seemingly insignificant methyl groups at different positions (Fig. 1b) of *N,N,N′,N′*-tetraarylbenzidine (TPD derivative) molecule can influence the hole-drift mobility therefore allowing desired customization of conjoined TPD fragments.[14]

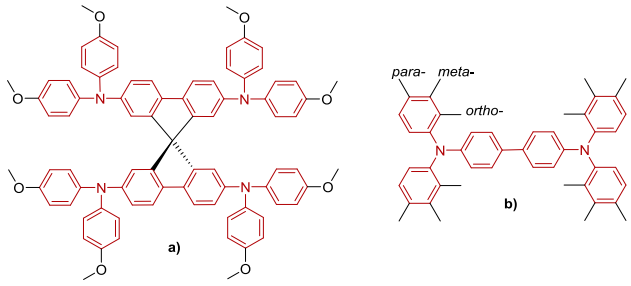

Figure 1. a) spiro-OMeTAD; b) TPD-type molecule with methyl groups at different positions.

The concept of conjoined TPDs also suggests to investigate alternative ways of connecting these compounds in non-planar manner and Tröger's base provides a valuable opportunity here. Tröger's base (TB) is V-shaped C_2-symmetric chiral molecule consisting of a bicyclic aliphatic methanodiazocine unit fused with two aromatic rings. Its structure allows it to be used as a core and provide angle orientation for the conjugated π-systems attached to it. Recent investigations have also revealed that rigidity of the TB scaffold and high molecular mass *via* its 2-fold functionalization impart crystallization, significantly increase glass transition temperature and render the TB derivatives highly amorphous and thermally stable.[15-17] Also our recently published

[a] T. Braukyla, Dr. M. Daskeviciene, Dr. T. Malinauskas, Prof. V. Getautis
Department of Organic Chemistry
Kaunas University of Technology
Radvilenu pl. 19, Kaunas, 50254, Lithuania
E-mail: tadas.malinauskas@ktu.lt, vytautas.getautis@ktu.lt
[b] Dr. N. Sakai, Prof. H. J. Snaith
Department of Physics
Clarendon Laboratory, University of Oxford
Parks Road, Oxford, OX1 3PU, UK
E-mail: henry.snaith@physics.ox.ac.uk
[c] E. Kamarauskas, Dr. V. Jankauskas
Department of Solid State Electronics
Vilnius University
Sauletekio 9, Vilnius, 10222, Lithuania
[d] Institute of Applied Research, Vilnius University, Saulėtekio 3, 10257, Vilnius, Lithuania
E-mail: regimantas.komskis@gmail.com, saulius.jursenas@tmi.vu.lt
† These authors have contributed equally.

Supporting information for this article is given via a link at the end of the document.

work on V-shaped HTMs containing TB core encourages further work in this field as presented compounds had comparatively high charge mobility, were fully amorphous, easily processable and demonstrated very good thermal and morphological stability.[18]

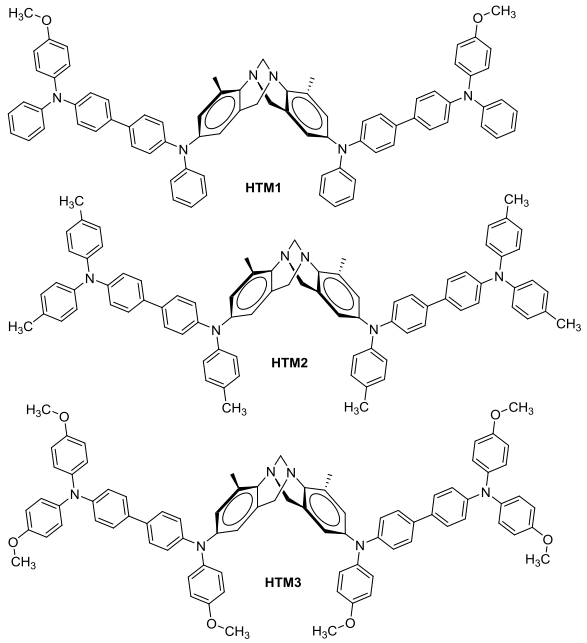

Figure 2. Compounds **HTM1**-**HTM3**.

In this paper, we report synthesis and properties of novel V-shaped charge transporting molecules **HTM1**-**HTM3** (Fig. 2) consisting of TPD-type moieties conjoined by Tröger's base core. These hole transporting materials, can be solution processed, demonstrate high glass transition temperatures and thermal stability and possess comparatively high charge drift mobility (up to 0.036 $cm^2 V^{-1} s^{-1}$).

Results and Discussion

The hole transporting materials **HTM1**, **HTM2** and **HTM3** have been synthesized by firstly obtaining intermediate biphenyl compounds, **2a, 2b and 2c** respectively**,** and then coupled with brominated Tröger's base[19] (Scheme 1).
Intermediate biphenyl compounds **1b and 1c** were synthesized from the 4,4'-dibromobiphenyl and respective aniline employing Buchwald-Hartwig cross-coupling reaction (respectively, commercially available **1a** was utilized); the next step of the same reaction with appropriate aryl halide was employed to obtain compounds **2a-2c**, which furthermore were used in palladium catalyzed C–N cross-coupling reaction with brominated Tröger's base to obtain investigated HTMs (**HTM1**-**HTM3**).

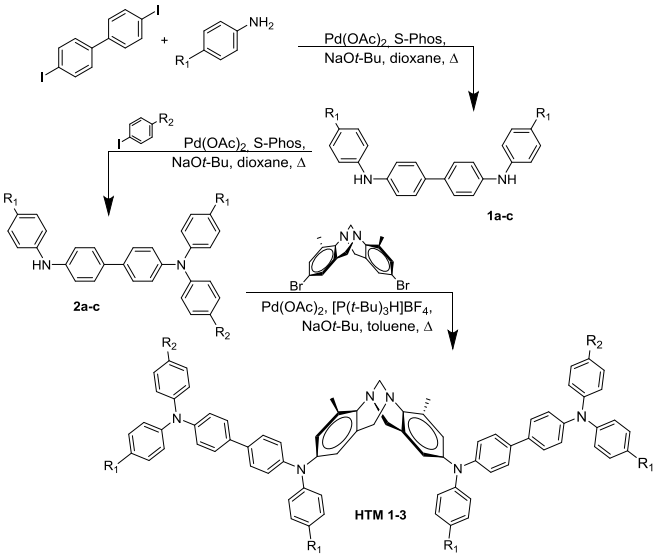

Scheme 1. Synthesis of **HTM1**-**HTM3,** where **1a, 2a, HTM1**: R_1=H, R_2=OCH_3; **1b, 2b, HTM2**: R_1=R_2=CH_3; **1c, 2c, HTM3**: R_1=R_2=OCH_3.

Structures of TB derivatives **HTM1**-**HTM3** were confirmed by NMR ^{1}H and ^{13}C spectroscopy as well as elemental analysis.
Pattern of the signals in the interval of 3.85-4.50 ppm in the ^{1}H NMR spectrum is essential for the methylene bridge identification, proving the presence of the TB core. Each ^{1}H NMR spectrum of **HTM1**-**HTM3** shows a doublet near each margin of the mentioned interval and these two doublets signify that the protons in bridging methylene part (Ar-CH_2-N) are magnetically nonequivalent due to the rigid structure of the TB.

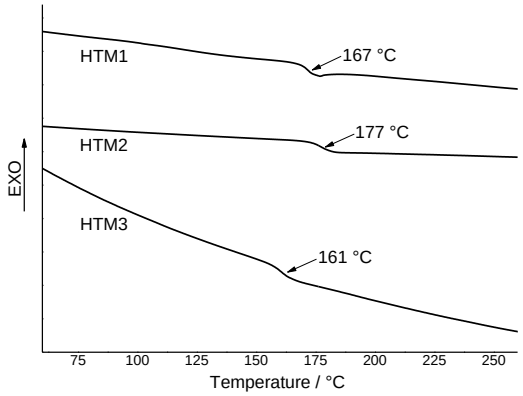

Figure 3. DSC second heating curves of **HTM1**-**HTM3** (heating rate 10 °C min^{-1}).

As a contrasting example to this, signals of two protons of the other bridging methylene carbon (N-CH_2-N) can be observed as a singlet at 4.30 or 4.31 ppm in these spectrums (Fig. S10, Fig. S12, Fig. S14).

Non-planar structure of TB and subsequently TPD-type fragments oriented angle-wise towards each other forming non-compact structural bulk hampers the crystallization processes in the investigated HTMs. Differential scanning calorimetry (DSC) measurements reveal that all investigated compounds **HTM1-HTM3** exist only in amorphous state. During the first heating a peak particularly specific to glass transition (T_g) can be observed at 171 °C and at 177 °C in **HTM1** and **HTM2** curves respectively and not so intensively in **HTM3** curve (Fig. S1-S3). No crystallization takes place during cooling or second heating scans and again only glass transition (T_g) is registered at 167°C, 177°C and 161°C in **HTM1, HTM2** and **HTM3** curves respectively (Fig. 3, Table 1).

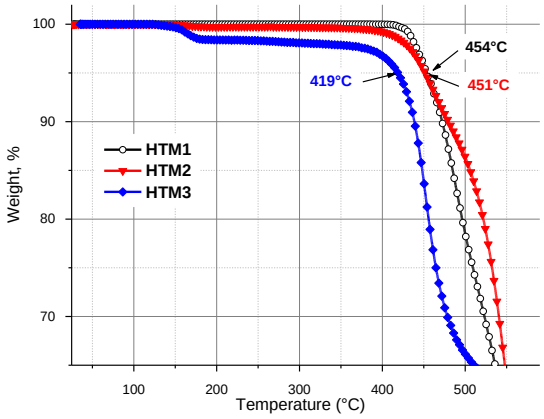

Figure 4. TGA curves for compounds **HTM1, HTM2** and **HTM3**.

Thermogravimetric analysis reveals high decomposition temperatures (Fig. 4, Table 1). Slight weight loss (up to ~2 %) observable for **HTM3** in Fig. 4 from ~130° is attributed to the evaporation of the traces of residual solvents that remained after purification of the material. In general, all the compounds within the series have demonstrated superior thermal stability, with initial destruction temperatures (corresponding to 5% weight loss) well exceeding 400 °C and are comparable to that of spiro-OMeTAD (440°C)[20] and even slightly exceeds it in cases of **HTM1** and **HTM2**, therefore confirming that materials are thermally stable and are promising candidates for practical applications.

UV – VIS absorption and emission spectra of Tröger`s base derivatives **HTM1**, **HTM2**, **HTM3** measured in THF, polystyrene (PS) film and neat film are shown in Fig. 5. **HTM1** – **HTM3** compounds show twofold absorption characteristics peaking at 303 nm – 305 nm and 354 nm – 355 nm, respectively what is typical feature of various triphenylamine-cored compounds.[21,22] All three compounds exhibit deep-blue structure-less emission peaked at 413 nm – 424 nm. Incorporation of triphenylamine side chains has a major impact on both absorption and emission properties of the molecules. Observed fluorescence redshift (of 10 nm) for the compound **HTM3** can be attributed to the polar nature of the metoxy substituents. Interestingly, all Tröger`s base derivatives **HTM1**, **HTM2** and **HTM3** show relatively high fluorescence quantum yield (45 to 52%) which can be due to restriction of the phenyl moiety torsion by bulky substituents.[23] This is supported by similar fluorescence properties of the compounds tested in a rigid PS matrix. Compounds exhibit strong room temperature phosphorescence recorded at 1 ms delay time after excitation (see Fig. 5). Estimated triplet state energy shifts from 2.37 eV to 2.35 eV and 2.34 eV for compounds **HTM1**, **HTM2** and **HTM3**, respectively. The triplet energy values are typical for TPA-cored compounds.[24,25] Close molecular packing of the Tröger`s base derivatives in the neat films resulted only in minor redshift of the fluorescence, indicating on restricted intermolecular interaction and exciton coupling (see Fig. 5). The fluorescence of the neat film for compound **HTM2** show additional broad excimer emission peaked at about 500 nm, which can be attributed to the absence of metoxy substituents.

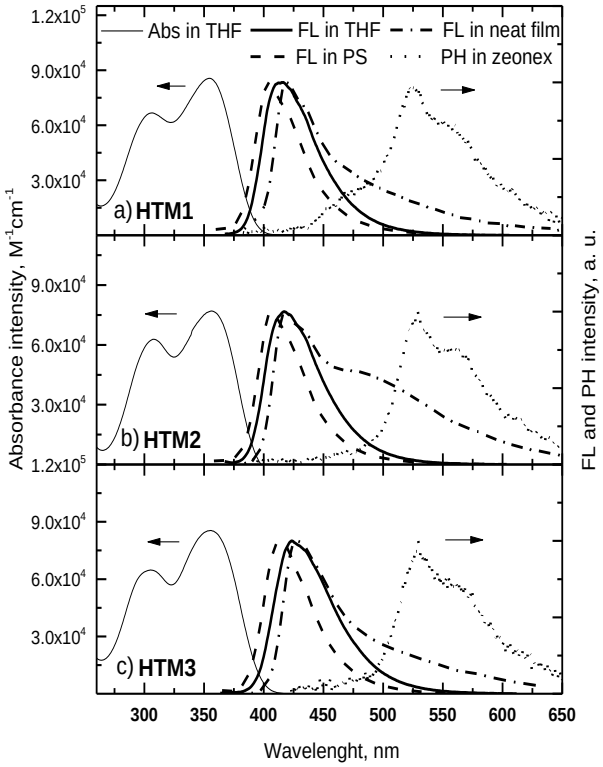

Figure 5. Absorbance (Abs) and emission (FL) spectra of Tröger`s base derivatives **HTM1** (**a**), **HTM2** (**b**), **HTM3** (**c**). Black line – absorption in THF (10^{-6} M^{-1}) solution, black bold line – fluorescence in THF solution, dash line – fluorescence in PS film (0.1 wt %), dash dot line – fluorescence in neat film, dot line – phosphorescence in Zeonex (1 wt %) film.

Table 1. Optical and thermal properties of **HTM1** – **HTM3** derivatives

Comp.	T_g [°C] [a]	T_{dec} [°C] [b]	THF solution				PS film 0.1 wt %		Neat film		Zeonex film 1 wt %
			λ_{abs} (nm) [c]	ε (l mol^{-1} cm^{-1}) [d]	λ_F (nm) [e]	Φ_F (%) [f]	λ_F (nm) [e]	Φ_F (%) [f]	λ_F (nm) [e]	Φ_F (%) [f]	λ_{PH} (nm) [g]
HTM1	167	454	304 354	66391 86250	413	44.5	403	42	418	2.3	523
HTM2	177	451	305 356	63454 77413	419	46.8	406	44.2	419	2.2	527
HTM3	161	419	303 355	65804 86485	424	52.1	413	50.2	428	3.9	529

[a] Determined by DSC: scan rate, 10 K/min; N_2 atmosphere; second run. [b] Onset of decomposition determined by TGA: heating rate, 10 K/min; N_2 atmosphere. [c] Absorption maxima in THF solution [d] Molar extinction coefficient of absorption in THF solution at peak positions [e] Fluorescence maxima in THF solution, PS film (0.1 wt %), neat film [f] Fluorescence quantum yield in THF solution, PS film, neat film [g] Phosphorescence maxima in Zeonex film (1 wt %)

To determine excited state relaxation dynamics fluorescence decay transient measurements were carried out (see Figure S16 and Table S1). All compounds demonstrate exponential fluorescence decay transients in THF solution with excited state decay constant 1.31 ns and 1.35 ns for compounds **HTM1** and **HTM2,** respectively and similar radiative recombination decay constant (2.88 ns and 2.94 ns for **HTM1** and **HTM2**, respectively). Incorporation of metoxy substituents enhances relaxation time slightly (up to 1.58 ns) for compound **HTM3** (see Table S1). Almost the same radiative recombination decay constant (3.03 ns) and slower nonradiative decay constant (3.30 ns) for **HTM3** implies to restriction of molecular torsions in phenylamine chains, what results in enhancement of the fluorescence quantum yield. The restriction of molecular torsions in a rigid polymer medium ensures faster fluorescence decay rate (0.99 ns – 1.08 ns) with exponetial decay dynamics and similar fluorescence quantum efficiency. Meanwhile, relaxation of excited state in neat films demonstrates nonexponential decay characteristics and reduced quantum efficiency (up to 3.9 %) due enhanced exciton migration and trapping to the nonradiative states.[26]

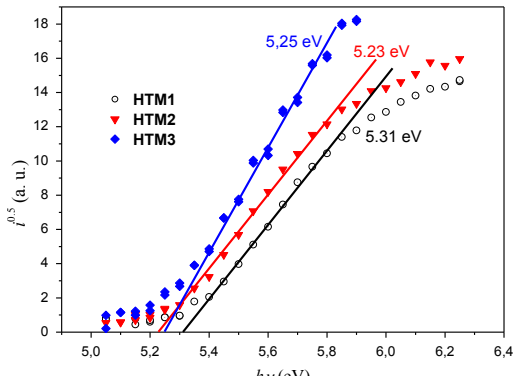

Figure 6. Photoemission in air spectra of **HTM1-HTM3**.

An understanding of solid state ionization potential (I_p) is fundamental when considering the use of an organic material for hole-transport applications as it can help in identifying suitable partner organic transport and inorganic electrode materials. The ionization potential was measured by the photoelectron spectroscopy in air (PESA) method (Figure 6) and results are presented in Table 2; the measurement error is evaluated as 0.03 eV. I_p values of compounds **HTM1–HTM3** displays the influence of methyl- and methoxy- group substituents in phenyl rings - while **HTM1** has four unsubstituted phenyl rings and highest I_p value of 5.31 eV, this value lowers down as all terminal phenyl rings gets *para*-substituted in **HTM2.** Moreover, it can be clearly seen, that incorporation of six donating metoxy- fragments in **HTM3** resulted in the lowest I_p within the series.

Table 2. Energy level and hole mobility data for **HTM1–HTM3** [a]

Comp.	E_g^{opt} [eV] [b]	E_{HOMO} [eV] [c]	E_{LUMO} [eV] [d]	I_p [eV] [e]	EA [eV] [f]	μ_0 [cm^2 V^{-1} s^{-1}] [g]	μ_h [cm^2 V^{-1} s^{-1}] [h]
HTM1	3.16	–5.23	–2.15	5.31	–2.07	4×10^{-8} *	4×10^{-6} *
HTM2	3.15	–4.92	–2.1	5.25	–1.77	1.2×10^{-4}	0.004
HTM3	3.13	–5.11	–2.1	5.23	–1.98	6×10^{-5}	0.036

[a] The CV measurements were carried out at a glassy carbon electrode in dichloromethane solutions containing 0.1 M tetrabutylammonium hexafluorophosphate as electrolyte and Pt wire as the reference electrode. Each measurement was calibrated with ferrocene (Fc). Potentials measured vs Fc+/Fc. [b] The optical band gaps E_g^{opt} estimated from the edges of electronic absorption spectra in solution. [c] Conversion factors: ferrocene in DCM vs SCE 0.46[27],SCE vs SHE: 0.244[28], SHE vs. vacuum: 4.43[29]. [d] E_{LUMO} calculated from the equation $E_{LUMO} = I_p - E_g^{otp}$ [e] Solid state ionization potential (I_p) was measured by the photoemission in air method from films. [f] EA calculated from the equation $EA = E_{HOMO} - E_g^{otp}$ [g] Mobility value at zero field strength. [h] Mobility value at 6.4×10^5 V cm^{-1} field strength.

*- **HTM1** mobility values were measured from the mixture of compound **HTM1** and PC-Z (1:1).

Ground-state oxidation potentials of the HTMs were measured employing the cyclic voltammetry (CV) technique (Table 2). These values do not represent any absolute solid-state or gas-phase ionization energies, but can be used to compare different compounds relative to one another. All three TB derivatives undergo reversible oxidation in their CV scans, indicating the electrochemical stability of the compounds (Fig. S4).

To further analyze charge transport properties of synthesized compounds **HTM1–HTM3** xerographic time-of-flight (XTOF) technique was used. Examples of mobility field dependencies are given in Fig. 7. The values of charge mobility defining parameters: zero field mobility (μ_0) and the mobility at the electric field of 6.4×10^5 V cm^{-1} for the compounds **HTM1–HTM3** are given in the Table 2. The room temperature hole-drift mobility of the methoxy-substituted **HTM3** was 0.036 cm^2 V^{-1} s^{-1} at strong electric fields

and it is approximately nine times higher than that of the methyl-substituted analogue **HTM2** which demonstrated intermediate performance and μ_h of 0.004 $cm^2 V^{-1} s^{-1}$ was reached. Even though in case of **HTM1** a mixture of compound and biphenol-Z polycarbonate (PC-Z) in weight ratio 1:1 was used in order to obtain the uniform layer and therefore expected result for the pure material should be one order of magnitude higher it still had charge mobility values in a range of 10^{-6} which illustrates adversely affects that four unsubstituted phenyl rings cause.

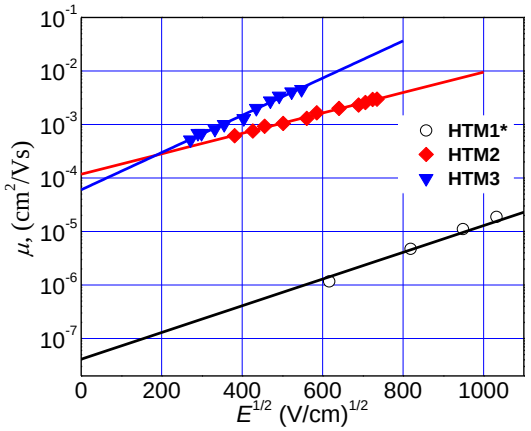

Figure 7. Electric field dependencies of the hole drift mobilities (μ) in the charge-transport layers of Tröger base derivatives **HTM1–HTM3**. In case of **HTM1** mixture of compound and PC-Z (1:1) was used.

Compared with other low molecular weight hole transporting materials,[30-35] synthesized TB derivatives **HTM2** and **HTM3** demonstrate comparatively high hole drift mobility. An interesting phenomenon was observed among these compounds as comparing methyl- and methoxy- substituted molecules this difference does not cause the decrease in charge mobility – which is usually a tendency in HTMs. On the other hand this phenomenon was also observed and mentioned in literature[36-38] where experimental data and theoretical calculations suggests that in case of some methoxy- substituted triphenylamine compounds (they share this structural feature with **HTM3**) despite the increased dipole moments enhancement of intramolecular interactions is observable making the positive impact to hole mobility of these compounds. On the other hand **HTM1** have much lower charge mobility – presumably caused by high dipole moment but with not enough methoxy groups to induce beneficial intramolecular interactions and therefore counterweight the negative effects as observed in **HMT3**.

I_p values of compounds **HTM1–HTM3** are in the rage of 5.31-5.23 eV and can be seen as a result of electron-donating methyl- and methoxy- groups – I_p values are decreasing with higher number of such substituents on phenyl rings – even more so then methoxy- group is used. Measured ionization potentials are not exceeding I_p value of perovskite (e.g. -5.4 eV) for methylammonium lead iodide ($FA_{0.83}Cs_{0.17}PbI_{2.55}Br_{0.45}$). This observation combined with very good charge transporting properties is suggesting that synthesized compounds are compatible with and can be used in fabrication of PSC.

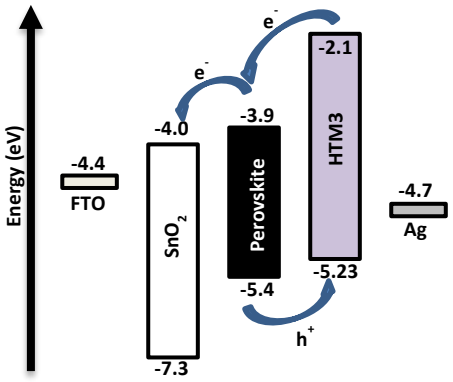

Figure 8. Energy level diagram for the PSC devices constructed using **HTM3**.

As the most promising property-wise among the synthesized TB derivatives **HTM3** have been preliminary tested as hole transporting semiconductor for the perovskite solar cells. The experiments were carried out using perovskite precursor containing a cation and anion mixture in a device stack of fluorine doped tin oxide(FTO)/compact SnO_2/C_{60}/ perovskite/HTM/Ag (Figure 8). All the fabrication details can be found in the experimental section.

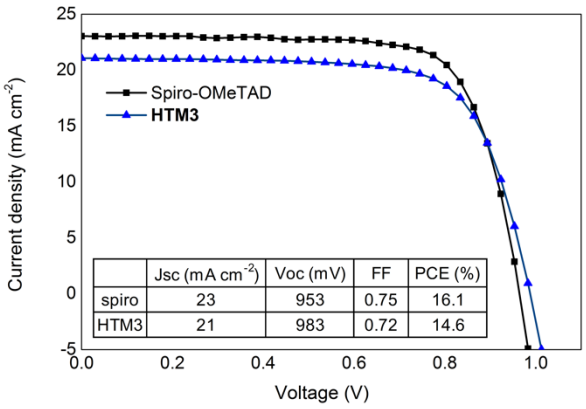

Figure 9. Best performing perovskite solar cells current density-voltage characteristics with **HTM3** and spiro-OMeTAD as hole transporting materials.

Respectable maximum power conversion efficiency of 14.6 % under AM 1.5 G illumination was recorded in the perovskite device containing **HTM3** as hole transporting material. The measured fill factor was 0.72, the current density (J_{sc}) 21.0 mA cm^{-2}, and the open-circuit voltage (V_{oc}) 983 mV (Figure 9). Spiro-OMeTAD) was used as a reference material and device from the same batch of solar cells, prepared following the same device fabrication

procedure, but using spiro as hole-extracting layer, displayed a PCE of 16.1%.

Conclusions

In conclusion, we have demonstrated synthesis procedure of merely three steps to obtain solution processable V-shaped hole transporting materials based on TPD-type moieties conjoined by a Tröger`s base core. TB core provides orientation to TPD fragments angle-wise towards each and hampers the crystallization processes making the compound amorphous, while substituted TPD-type moieties provide high charge mobility and desired electrical properties. Investigated hole transporting materials are promising candidates for application in organic and hybrid optoelectronic devices as they can be handled in air, are amorphous and require no high temperature annealing steps, have high glass transition temperatures, can be solution deposited, and possess comparatively high mobility (up to 0.036 $cm^2 V^{-1} s^{-1}$).

Experimental Section

Materials and General Procedures

All chemicals were purchased from Aldrich and used as received without further purification. 2,8-Dibromo-4,10-dimethyl-6*H*,12*H*-5,11-methanodibenzo[*b,f*][1,5]diazocine (**1**) was synthesized according to the procedure reported earlier.[39] ^{1}H NMR spectra were recorded at 400 MHz on a Bruker Avance III spectrometer with a 5 mm double resonance broad band BBO z-gradient room temperature probe, ^{13}C NMR spectra were collected using the same instrument at 100 MHz. The chemical shifts, expressed in ppm, were relative to tetramethylsilane (TMS). All the experiments were performed at 25 °C. The course of the reactions products were monitored by TLC on ALUGRAM SIL G/UV254 plates and developed with I_2 or UV light. Silica gel (grade 62, 60–200 mesh, 150 Å, Aldrich) was used for column chromatography. Diatomaceous earth (Celite® 500 fine, Sigma-Aldrich) was used for filtering where mentioned. Elemental analysis was performed with an Exeter Analytical CE-440 Elemental. Differential scanning calorimetry (DSC) was performed on a Q10 calorimeter (TA Instruments) at a scan rate of 10 K min^{-1} in the nitrogen atmosphere. The glass transition temperatures for the investigated compounds were determined during the second heating scan. Thermogravimetric analysis (TGA) was performed on a Q50 thermogravimetric analyser (TA Instruments) at a scan rate of 10 K min^{-1} in the nitrogen atmosphere.

Optical properties

For optical measurements, the dilute solutions of the investigated compounds were prepared by dissolving them in a spectral grade THF) at 1×10^{-6} M concentration. The PS films with the dispersed compounds with 0.1 wt % concentration were prepared by mixing the dissolved compounds and PS in THF solutions at appropriate ratios and casting the solutions on quartz substrates under ambient conditions. For phosphorescence measurements, Zeonex (polyolefin) polymer and spectral grade chlorobenzene as a solvent with dispersed compounds of 1 % w.t. in wet casted films under ambient conditions were used. The neat films of the compounds were casted from 1×10^{-3} M THF solutions under ambient conditions. Absorption spectra of the dilute THF solutions were recorded on a UV – VIS – NIR spectrophotometer Lambda 950 (Perkin Elmer). Fluorescence of the investigated compounds in dilute THF solutions, PS and neat films was measured using excitation at 350 nm from a Xe lamp (FWHM<10 meV) using a back-thinned CCD spectrometer PMA-11 (*Hamamatsu*). Fluorescence quantum yields (Φ_F) of the solutions, PS and neat films were estimated using the integrated sphere method with integrating sphere (*Sphere Optics*) coupled to the CCD spectrometer via optical fiber using 350 nm excitation wavelength. Quinine sulfate in 0.1 M H_2SO_4 with Φ_F 0.53 ± 0.023 was used as a reference. Fluorescence transients were measured using a time-correlated single photon counting system PicoHarp 300 (*PicoQuant*) utilizing a semiconductor diode (repetition rate 1 MHz, pulse duration 70 ps, emission wavelength 350 nm) as an excitation source. Radiative (τ_r) and nonradiative (τ_{nr}) decay time constants were calculated using the following relations: $\tau_F = \tau_F/\Phi_F$, $\tau_{nr} = \tau_F/(1-\Phi_F)$ where the term τ_{nr} takes into account all the possible nonradiative decay pathways. Phosphorescence measurements of 1 % w.t. Zeonex (polyolefin) films were performed using nanosecond (τ = 7 ns) Ekspla NT 242 laser with 350 nm excitation (laser fluence 200 μJ) and Andor Sr-303i-A iCCD camera at 5×10^{-5} mbar vacuum by closed-cycle helium cryostat (293 K) with 1 ms delay time after excitation.

Cyclic Voltammetry

CV measurements were carried out by a three-electrode assembly cell from Bio-Logic SAS potentiostat-galvanostat. The measurements were carried out at a glassy carbon electrode in dichlormethane solutions containing 0.1 M tetrabutylammonium hexafluorophosphate as electrolyte, Pt as the reference and counter electrodes at a scan rate of 50 mV s^{-1}. Each measurement was calibrated with ferrocene (Fc). Oxidation potential was obtained as an average value between anodic and cathodic potentials: $E_{1/2}^{red/ox} = 1/2(E_{pc} + E_{pa})$.

Ionization Potential Measurements

The solid state ionization potential (I_p) of the layers of the synthesized compounds was measured by the electron photoemission in air method. The samples for the ionization energy measurement were prepared by dissolving materials in THF and were coated on Al plates pre-coated with ~0.5 μm thick methylmethacrylate and methacrylic acid copolymer adhesive layer. The thickness of the transporting material layer was 0.5-1 μm. Usually the photoemission experiments are carried out in vacuum and high vacuum is one of the main requirements for these measurements. If vacuum is not high enough the sample surface oxidation and gas adsorption are influencing the measurement results. In our case, however, the organic materials investigated are stable enough to oxygen and the measurements may be carried out in the air. The samples were illuminated with monochromatic light from the quartz monochromator with deuterium lamp. The power of the incident light beam was $(2\text{-}5)\cdot10^{-8}$ W. The negative voltage of –300 V was supplied to the sample substrate. The counter-electrode with the 4.5x15 mm^2 slit for illumination was placed at 8 mm distance from the sample surface. The counter-electrode was connected to the input of the BK2-16 type electrometer, working in the open input regime, for the photocurrent measurement. The 10^{-15} – 10^{-12} A strong photocurrent was flowing in the circuit under illumination. The photocurrent I is strongly dependent on the incident light photon energy hν. The $I^{0.5} = f(h\nu)$ dependence was plotted. Usually the dependence of the photocurrent on incident light quanta energy is well described by linear relationship between $I^{0.5}$ and $h\nu$ near the threshold.[40,41] The linear part of this dependence was extrapolated to the hν axis and I_p value was determined as the photon energy at the interception point.

Hole Drift Mobility Measurements

The samples for the hole mobility measurements were prepared by spin-coating the solutions of the of the synthesized compounds or compositions of synthesized compounds with bisphenol-Z polycarbonate (PC-Z) (Iupilon

Z-200 from Mitsubishi Gas Chemical Co.) in weight ratio 1:1 on the polyester films with conductive Al layer. The layer thickness was in the range 5-10 μm. The hole drift mobility was measured by xerographic time of flight technique (XTOF).[42-44] Electric field was created by positive corona charging. The charge carriers were generated at the layer surface by illumination with pulses of nitrogen laser (pulse duration was 2 ns, wavelength 337 nm). The layer surface potential decrease as a result of pulse illumination was up to 1-5 % of initial potential before illumination. The capacitance probe that was connected to the wide frequency band electrometer measured the speed of the surface potential decrease dU/dt. The transit time t_t was determined by the kink on the curve of the dU/dt transient in double logarithmic scale. The drift mobility was calculated by the formula $\mu = d^2/U_0 t_t$, where d is the layer thickness, U_0 – the surface potential at the moment of illumination.

Perovskire Device Fabrication and Measurements

FTO-coated glass sheets (TEC 15, 15Ω/sheet, Pilkington) were etched with zinc powder and 2M HCl to obtain the required electrode pattern. The sheets were then washed with 2% Hellmanex in water, deionized water, acetone, ethanol and iso-propanol. The last traces of organic residues were removed by oxygen plasma cleaning for 10 min. The FTO sheets were subsequently coated with a SnO_2 compact layer with 40 mM Aquarius $SnCl_4 \cdot 5H_2O$ solution at 70 °C for 60 min then washed with DI-water and ethanol. The coated FTO substrate was then heated at 180 °C for 60 min. C60 (10 mg/ml in 1,2, di-chlorobenzene) was coated on SnO_2 compact layer at 2000 rpm for 40 sec. C60 between the perovskite and the TiO_2 contact is needed to shift the perovskite valence band to lower binding energies.[45] 1.2 M perovskite precursor solutions were made by FAI, CsI, PbI_2 and $PbBr_2$ to obtain a stoichiometric solution with desired composition i.e. $FA_{0.83}CsI_{0.17}PbI_{2.55}Br_{0.45}$ dissolving in dimethylformamide (dehydrate DMF). 70 ul of HI and 30 ul of HBr were added into 1 ml of perovskite solution. After the addition of acids, the solution was stirred for 40 h. Perovskite precursor solution was coated onto the SnO_2/C60 by a consecutive two-step spin-coating process at 1300 rpm for 20 sec and 3000 rpm for 20 sec under low humidity (7-12% at 20°C) condition with a dry compressed air parching in dry box. The perovskite films were quickly dried by the compressed air blowing for 30 sec for drying the film surface. The perovskite films were drying at 20-25 °C for 15 min and then 70 °C for 15 min on the hot plate. The dried films were annealing at 180 °C for 90 min in the box oven without controlling humidity. 40 mg HTM containing TB core (**HTM3**) was solved in 1 ml cholobenzene with additives of 30 μl tert-butylpyridine, 10 μl lithium bis(trifluoromethylsulfonyl)imide salt in acetonitrile (510 mg ml^{-1}) and 17 μl and 20 μl $Co[t\text{-}BuPyPz]_3[TFSI]_3$ in acetonitrile (50mg ml^{-1}). The HTM solution was coated on the perovskite with spin-coating at 3500 rpm for 30 sec. 87 mg spiro-OMeTAD as a reference was solved in 1 ml cholobenzene with additives of 30 μl tert-butylpyridine and 10 μl lithium bis(trifluoromethylsulfonyl)imide salt in acetonitrile (510 mg ml^{-1}). The spiro-OMeTAD solution was coated on the perovskite with spin-coating at 2500 rpm for 45 sec. 50-80 nm Ag metal contact layer was deposited as the counter electrode on the HTM layer by thermal evaporation.

The cell performance evaluated by the current–voltage (*J-V*) measurements under simulated solar light (AAB ABET technologies Sun 2000 solar simulator) with its light intensity, 100 mW cm^{-2} (AM 1.5), calibrated against a standard amorphous-silicon PV cell (NREL-calibrated KG5 filtered silicon reference cell). The *J-V* curves were measured by short circuit (0 V) to forward bias (-1.4V) and forward bias (-1.4V) to short circuit (0 V). The cell aperture area of light incidence was set to 0.0913 cm^2 photoactive area.

***N*⁴-(4-methoxyphenyl)-*N*⁴,*N*⁴'-diphenyl-[1,1'-biphenyl]-4,4'-diamine (2a)**

2-Dicyclohexylphosphino-2′,6′-dimethoxybiphenyl (SPhos) (0.0554 g, 0.135mmol) (0.015equiv.) and palladium (II) acetate (0.0101g, 0.045mmol) (0.005equiv.) were dissolved in dioxane (9 mL, 3mL per gram of *N,N*-diphenylbenzidine) under argon atmosphere and stirred at 80°C for 5min, *N,N*-diphenylbenzidine (3.028 g, 9 mmol), 4-iodoanisole (2.106 g, 9 mmol) (1 equiv.) and sodium *tert*-butoxide (1.2109 g, 12.6 mmol) (1.4 equiv.) were added and the mixture was heated at reflux for 3 hours. After termination of the reaction the solution was extracted with ethyl acetate. The organic layer was dried over anhydrous Na_2SO_4, filtered, solvent was removed and the residue purified by column chromatography (THF/*n*-hexane 1/24, *v*/*v*) to give whitish solid product. Yield: 45% (1.78 g).

***N*⁴,*N*⁴'-di-*p*-tolyl-[1,1'-biphenyl]-4,4'-diamine (1b)**

2-Dicyclohexylphosphino-2′,6′-dimethoxybiphenyl (SPhos) (0.0985 g, 0.240 mmol) (0.03 equiv.) and palladium (II) acetate (0.0180 g, 0.080 mmol) (0.01 equiv.) were dissolved in dioxane (16.3 mL, 5mL per gram of 4,4'-diiodobiphenyl) and stirred under argon atmosphere at 80°C for 10min, 4,4'-diiodobiphenyl (3.2480 g, 8 mmol), *p*-toluidine (1.7573 g, 16.4 mmol) (2.05 equiv.) and sodium *tert*-butoxide (2.1526g, 22.40 mmol) (2.8 equiv.) were added and the mixture was heated at reflux for an hour. After termination of reaction the mixture was diluted with THF and filtered through Celite. Solvent was removed, residue dissolved in ~20ml of hot THF, ~4ml of *n*-hexane was being slowly added dropwise until crystallization started. Mixture was left to cool down; crystals were filtered and washed with *n*-hexane to give fine white crystals (75 %, 2.2 g). ^{1}H NMR (400 MHz, DMSO-d_6) δ 8.06 (s, 2H), 7.45 (d, J = 8.5 Hz, 4H), 7.10 – 6.97 (m, 12H), 2.23 (s, 6H). ^{13}C NMR (101 MHz, DMSO-d_6 + Chloroform-*d*) δ 129.79, 129.68, 129.10, 126.71, 126.59, 117.91, 116.78, 116.66, 20.77. Calcd. for $C_{26}H_{24}N_2$ (%): C 85.68; H 6.64; N 7.69. Found (%): C 85.97; H 6.35; N 7.68.

***N*⁴,*N*⁴,*N*⁴'-tri-*p*-tolyl-[1,1'-biphenyl]-4,4'-diamine (2b)**

2-Dicyclohexylphosphino-2′,6′-dimethoxybiphenyl (SPhos) (0.0456g, 0.111 mmol) (0.015 equiv.) and palladium (II) acetate (0.0083 g, 0.037 mmol) (0.005 equiv.) were dissolved in dioxane (15 mL, 5.5mL per gram of **1b**) under argon atmosphere and stirred at 80°C for 5min, *N*⁴,*N*⁴'-di-*p*-tolyl-[1,1'-biphenyl]-4,4'-diamine (**1b**) (2.6972 g, 7.4 mmol), 4-iodtoluene (1.6134 g, 7.4 mmol) (1 equiv.) and sodium *tert*-butoxide (1.00 g, 10.36 mmol) (1.4 equiv.) were added and the mixture was heated at reflux for 5 hours. After termination of reaction the mixture was diluted with THF and filtered through Celite, solvent was removed and the residue purified by column chromatography (acetone/*n*-hexane 1/24, *v*/*v*). Yield: 38% (1.27 g)

***N*⁴,*N*⁴'-bis(4-methoxyphenyl)-[1,1'-biphenyl]-4,4'-diamine (1c)**

2-Dicyclohexylphosphino-2′,4′,6′-triisopropylbiphenyl (XPhos) (0.2288 g, 0.480 mmol) (0.03 equiv.) and palladium (II) acetate (0.0359 g, 0.160 mmol) (0.01 equiv.) were dissolved in dioxane (32.8 mL, 6.5mL per gram of 4,4'-dibromobiphenyl) and stirred under argon atmosphere at 80°C for 10min, 4,4'-dibromobiphenyl (4.992 g, 16 mmol), *p*-anisidine (4.040 g, 16.4 mmol) (2.05 equiv.) and sodium *tert*-butoxide (4.305 g, 44.80 mmol) (2.8 equiv.) were added and the mixture was heated at reflux for 3 hours. After termination of reaction the mixture was diluted with THF and filtered through Celite passivated with 2% TEA solution in THF. Solvent was removed, residue dissolved in hot THF (~60mL) and ~20mL ethyl acetate was added. Solvent was being slowly evaporated until crystallization started. Mixture was left to cool down; crystals were filtered and washed with /n-hexane to give fine white crystals (72 %, 4.54 g).

***N*⁴,*N*⁴,*N*⁴'-tris(4-methoxyphenyl)-[1,1'-biphenyl]-4,4'-diamine (2c)**

2-Dicyclohexylphosphino-2′,6′-dimethoxybiphenyl (SPhos) (0.0677 g, 0.165mmol) (0.015 equiv.) and palladium (II) acetate (0.0123 g,

0.055mmol) (0.005 equiv.) were dissolved in dioxane (35 mL, 8mL per gram of **1c**) under argon atmosphere and stirred at 80°C for 5min, *N*^{4},*N*$^{4'}$-bis(4-methoxyphenyl)-[1,1'-biphenyl]-4,4'-diamine (**1c**) (4.3614 g, 11 mmol), 4-iodoanisole (2.5743 g, 11 mmol) (1 equiv.) and sodium *tert*-butoxide (1.4799 g, 15.4 mmol) (1.4 equiv.) were added and the mixture was heated at reflux for 3 hours. After termination of reaction the mixture was diluted with THF and filtered through Celite passivated with 2% TEA solution in THF, solvent was removed and the residue purified by column chromatography (THF/*n*-hexane 1/30, *v*/*v*) (silica gel in column was passivated with 2% TEA solution in THF beforehand) to give greyish prowder. Yield: 41.1% (2.27 g) ^{1}H NMR (400 MHz, Chloroform-*d*) δ 7.44 – 7.32 (m, 4H), 7.12 – 7.02 (m, 7H), 7.01 – 6.93 (m, 3H), 6.90 – 6.78 (m, 7H), 3.79 (m, 9H). Elemental analysis. Calcd. for $C_{33}H_{30}N_2O_3$ (%): C 78.86; H 6.02; N 5.57. Found (%): C 78.59; H 6.15; N 5.46.

_N_^{4},_N_$^{4'}$-(4,10-dimethyl-6_H_,12_H_-5,11-methanodibenzo[_b,f_][1,5]diazocine-2,8-diyl)bis(N$^{4'}$-(4-methoxyphenyl)-_N_^{4},_N_$^{4'}$-diphenyl-[1,1'-biphenyl]-4,4'-diamine) (HTM1)

2,8-dibromo-4,10-dimethyl-6*H*,12*H*-5,11-methanodibenzo[*b,f*][1,5]diazocine (**1**) (0.2842 g, 0.7 mmol) and *N*^{4}-(4-methoxyphenyl)-*N*^{4},*N*$^{4'}$-diphenyl-[1,1'-biphenyl]-4,4'-diamine (**2a**) (0.9294 g, 2.1 mmol) (3 equiv.) were dissolved in toluene (20 mL per gram of **1**) and stirred under argon atmosphere for 30min, tri-*tert*-butylphosphonium tetrafluoroborate (0.0055 g, 0.019 mmol) (0.027 equiv.) and palladium (II) acetate (0.0031 g, 0.014 mmol) (0.02equiv.) were added and mixture was stirred for 10 minutes, sodium *tert*-butoxide (0.2018 g, 2.100 mmol) (3 equiv.) was added and the mixture was heated at reflux for 6 hours. After termination of reaction the mixture was diluted with THF and filtered through Celite, solvent was removed and the residue purified by column chromatography (THF/toluene/*n*-hexane 1:19:30, *v*/*v*) to give greyish powder. Yield: 61% (0.483 g) ^{1}H NMR (400 MHz, Chloroform-*d*) δ 7.45 – 7.36 (m, 8H), 7.26 – 7.17 (m, 8H), 7.10 (d, *J* = 2.2 Hz, 2H), 7.09 – 7.02 (m, 18H), 7.01 – 6.92 (m, 4H), 6.89 – 6.80 (m, 6H), 6.55 (d, *J* = 2.5 Hz, 2H), 4.47 (d, *J* = 17.0 Hz, 2H), 4.30 (s, 2H), 3.87 (d, *J* = 17.0 Hz, 2H), 3.80 (s, 6H), 2.27 (s, 6H). ^{13}C NMR (101 MHz, $CDCl_3$) δ 156.23, 148.02, 147.83, 147.05, 146.71, 140.64, 134.05, 133.91, 129.19, 129.12, 127.35, 127.16, 127.14, 125.34, 123.99, 123.82, 123.07, 122.84, 122.45, 122.00, 120.21, 114.80, 55.50, 54.94, 29.72, 17.11. Calcd. for $C_{79}H_{66}N_6O_2$ (%):C 83.86; H 5.88; N 7.43. Found (%):C 83.94; H 6.07; N 7.13.

_N_^{4},_N_$^{4'}$-(4,10-dimethyl-6_H_,12_H_-5,11-methanodibenzo[_b,f_][1,5]diazocine-2,8-diyl)bis(_N_^{4},_N_$^{4'}$,_N_$^{4'}$-tri-_p_-tolyl-[1,1'-biphenyl]-4,4'-diamine) (HTM2)

2,8-dibromo-4,10-dimethyl-6*H*,12*H*-5,11-methanodibenzo[*b,f*][1,5]diazocine **(1)** (0.3654 g, 0.90 mmol) and *N*^{4},*N*^{4},*N*$^{4'}$-tri-*p*-tolyl-[1,1'-biphenyl]-4,4'-diamine (**2b**) (1.2275 g, 2.70 mmol) (3 equiv.) were dissolved in toluene (20 mL per gram of **1**) and stirred under argon atmosphere for 30min, tri-*tert*-butylphosphonium tetrafluoroborate (0.0071 g, 0.024 mmol) (0.027 equiv.) and palladium (II) acetate (0.0040 g, 0.018 mmol) (0.02equiv.) were added and mixture was stirred for 10 minutes, sodium *tert*-butoxide (0.2595 g, 2.70 mmol) (3 equiv.) was added and the mixture was heated at reflux for 6 hours. After termination of reaction the mixture was diluted with THF and filtered through Celite, solvent was removed and the residue purified by column chromatography (ethyl acetate/toluene/*n*-hexane 1:30:19, *v*/*v*) to give greyish powder. 42.4% (0.441 g) ^{1}H NMR (400 MHz, Chloroform-*d*) δ 7.42 – 7.35 (m, 8H), 7.10 – 6.96 (m, 32H), 6.83 (d, *J* = 2.5 Hz, 2H), 6.53 (d, *J* = 2.5 Hz, 2H), 4.46 (d, *J* = 16.8 Hz, 2H), 4.31 (s, 2H), 3.87 (d, *J* = 16.8 Hz, 2H), 2.31 (s, 18H), 2.27 (s, 6H). ^{13}C NMR (101 MHz, $CDCl_3$) δ 147.06, 145.31, 145.13, 134.08, 134.03, 133.92, 133.85, 132.62, 132.42, 129.93, 129.86, 129.82, 127.09, 127.06, 124.86, 124.54, 123.17, 122.93, 65.71, 54.93, 20.87, 20.83, 17.13. Calcd. for $C_{83}H_{74}N_6$ (%): C 86.27; H 6.46; N 7.27. Found (%): C 86.19; H 6.76; N 7.05.

_N_^{4},_N_$^{4'}$-(4,10-dimethyl-6_H_,12_H_-5,11-methanodibenzo[_b,f_][1,5]diazocine-2,8-diyl)bis(_N_^{4},_N_$^{4'}$,_N_$^{4'}$-tris(4-methoxyphenyl)-[1,1'-biphenyl]-4,4'-diamine) (HTM3)

2,8-dibromo-4,10-dimethyl-6*H*,12*H*-5,11-methanodibenzo[*b,f*][1,5]diazocine **(1)** (0.7265 g, 1.78 mmol) and *N*^{4},*N*^{4},*N*$^{4'}$-tris(4-methoxyphenyl)-[1,1'-biphenyl]-4,4'-diamine (**2c**) (2.2366 g, 4.45 mmol) (2.5 equiv.) were dissolved in toluene (20 mL per gram of **1**) and stirred under argon atmosphere for 30min, tri-*tert*-butylphosphonium tetrafluoroborate (0.0139 g, 0.048 mmol) (0.027 equiv.) and palladium (II) acetate (0.0080 g, 0.036 mmol) (0.02equiv.) were added and mixture was stirred for 10 minutes, sodium *tert*-butoxide (0.4276 g, 4.45 mmol) (2.5 equiv.) was added and the mixture was heated at reflux for 6 hours. After termination of reaction the mixture was diluted with THF and filtered through Celite passivated with 2% TEA solution in THF, solvent was removed and the residue purified by column chromatography (ethyl acetate/toluene/*n*-hexane 1:5:6 and ethyl acetate/toluene 1:24, *v*/*v*) (silica gel in column was passivated with TEA beforehand) to give greyish powder. 34% (0.733 g). ^{1}H NMR (400 MHz, Chloroform-*d*) δ 7.40 – 7.31 (m, 8H), 7.11 – 7.02 (m, 12H), 7.06 – 6.91 (m, 8H), 6.87 – 6.77 (m, 14H), 6.49 (d, *J* = 2.5 Hz, 2H), 4.46 (d, *J* = 16.9 Hz, 2H), 4.30 (s, 2H), 3.85 (d, *J* = 16.9 Hz, 2H), 3.79 (m, 18H), 2.26 (s, 6H). ^{13}C NMR (101 MHz, $CDCl_3$) δ 156.06, 155.74, 147.54, 146.97, 141.04, 140.70, 133.84, 132.87, 132.84, 131.13, 128.35, 127.26, 126.94, 126.42, 126.03, 124.13, 122.39, 121.27, 121.04, 119.01, 114.74, 114.67, 108.78, 67.74, 55.51, 55.48, 54.99, 17.14. Calcd. for $C_{83}H_{74}N_6O_6$ (%):C 79.65; H 5.96; N 6.72. Found (%):C 79.74; H 6.2; N 6.47.

Acknowledgements

The authors acknowledge funding from the European Union Seventh Framework Programme [FP7/2007-2013] under grant agreement No. 604032 of the MESO project and Research Council of Lithuania (grant No. MIP-105/2015).

1. IEA. Technology Roadmap Solar Photovoltaic Energy http://www.iea.org/publications/freepublications/publication/TechnologyRoadmapSolarPhotovoltaicEnergy_2014edition.pdf (accessed July 17, 2016).
2. Krebs, F. C.; Tromholt, T.; Jorgensen, M., Nanoscale **2010**, 2, 873−886.
3. NREL. Best Research-Cell Efficiencies http://www.nrel.gov/ncpv/images/efficiency_chart.jpg (accessed July 17, 2016).
4. J. Burschka, A. Dualeh, F. Kessler, E. Baranoff, N. L. Cevey-Ha, C. Yi, M. Nazeeruddin, and M. Grätzel, *J. Am. Chem. Soc.* **2011**, 133, 18042.
5. C. Jäger, R. Bilke, M. Heim, D. Haarer, H. R. Karickal, and M. Thelakkat, SPIE Proceedings **2001**, 4108, 104.
6. H.-S. Kim, C.-R. Lee, J.-H. Im, K.-B. Lee, T. Moehl, A. Marchioro, S.-J. Moon, R. Humphry-Baker., J.-H. Yum, J. E. Moser, M. Grätzel and N.-G. Park, Sci. Rep. **2012**, 5, 591.
7. H. Zhou, Q. Chen, G. Li, S. Luo, T. B. Song, H. S. Duan, Z. Hong, J. You, Y. Liu, and Y. Yang, Science **2014**, 345, 542.
8. H. Nishimura, N. Ishida, A. Shimazaki, A. Wakamiya, A. Saeki, L.T. Scott, and Y. Murata, *J. Am. Chem. Soc.* **2015**, 137 (50), 15656.
9. N. Marinova, W. Tress, R. Humphry-Baker, M. I. Dar, V. Bojinov, S. M. Zakeeruddin, M. K. Nazeeruddin, and M. Grätzel, ACS Nano. **2015**, 9 (4), 4200.
10. Y.S. Kwon, J. Lim, I. Song, I.Y. Song, W.S. Shin, S.-J. Moon, T. Park, J. Mater. Chem. **2012**, 22 (17), 8641.
11. J. Burschka, A. Dualeh, F. Kessler, E. Baranoff, N. L. Cevey-Ha, C. Yi, M. Nazeeruddin, and M. Grätzel, *J. Am. Chem. Soc.* **2011**, 133, 18042.
12. S. Ma, H. Zhang, N. Zhao, Y. Cheng, M. Wang, Y. Shen and G. Tu, J. Mater. Chem. A, **2015**, **3**, 12139-12144.
13. T. P. Saragi, T. Spehr, A. Siebert, T. Fuhrmann-Lieker, and J. Salbeck, Chem. Rev. **2007**, 107, 1011.
14. K. Nukada, K. Sato and Y. Akasaki, Electrophotography 1991, 30, 16.
15. I. Neogi, S. Jhulki, M. Rawat, R. S. Anand, T. J. Chow, J. N. Moorthy, *RSC Adv.*, **2015**, **5**, 26806.
16. I. Neogi, S. Jhulki, A. Ghosh, T. J. Chow, J. N. Moorthy, *ACS Appl. Mater. Interfaces*, **2015**, **7**, 3298−3305.

17. I. Neogi, S. Jhulki, A. Ghosh, T. J. Chow, J. N. Moorthy, *Org. Electron.,* **2014**, 15, 3766−3772.
18. T. Braukyla, N. Sakai, M. Daskeviciene, V. Jankauskas, E.Kamarauskas, T. Malinauskas, H. J. Snaith, V. Getautis, *Chem Asian J.* **2016**, 11, 2049-2056.
19. J. Jensen, K. Wärnmark, Synthesis **2001**, 12, 1873–1877.
20. T. P. Saragi, T. Spehr, A. Siebert, T. Fuhrmann-Lieker, and J. Salbeck, *Chem. Rev*. **2007**, 107, 1011.
21. M. Cekaviciute, J. Simokaitiene, V. Jankauskas, S. Raisys, K. Kazlauskas, S. Jursenas, J. V. Grazulevicius*. The Journal of Physical Chemistry C* **2013** 117, 7973–7980
22. T. Malinauskas, M. Daskeviciene, G. Bubniene, I. Petrikyte, S. Raisys, K. Kazlauskas, V. Gaidelis, V. Jankauskas, R. Maldzius, S. Jursenas, V. Getautis*. Chemistry - A European Journal* **2013** 19, 15044–15056
23. R. R. Reghu, J, Simokaitiene, J. V. Grazulevicius, S. Raisys, K. Kazlauskas, S. Jursenas, V. Jankauskas, A. Reina*, Dyes and Pigments* **2015** 115, 135–142
24. G. C. Terry, V. E. Uffindel, F. W. Wilets, Triplet state of triphenylamine, Nature vol. **1969** 223
25. S. A. Bagnich, S. Athanasopoulos, A. Rudnick, P. Schroegel, I. Bauer, N. C. Greenham, P. Strohriegl, A. Köhler. *The Journal of Physical Chemistry C* **2015** 119, 2380–2387
26. S. Raisys, K. Kazlauskas, M. Daskeviciene, T. Malinauskas, V. Getautis, S. Jursenas. *Journal of Materials Chemistry C* **2014** 2, 4792
27. N. Connelly, W. Geiger, *Chem. Rev***. 1996**, *96*, 877-910.
28. V. Pavlishchuk, A. Addison*, Inorganica Chimica Acta* **2000**, *298*, 97-102.
29. H. Reiss, A. Heller, *J. Phys. Chem.* **1985**, *89*, 4207-4213.
30. S. Allard, M. Forster, B. Souharce, H. Thiem, U. Scherf, Angew. *Chem. Int. Ed*. **2008**, 47, 4070−4098.
31. H. Reiss, A. Heller, *J. Phys. Chem.* **1985**, *89*, 4207–4213.
32. P. Baronas, K. Kazlauskas, A. Gruodis, V. Jankauskas, A. Tomkeviciene, J. Simokaitiene, J. V. Grazulevicius, S. Jursenas, *J. Lumin.* **2016**, *169*, 256–265.
33. T. Malinauskas, M. Daskeviciene, G. Bubniene, I. Petrikyte, S. Raisys, K. Kazlauskas, V. Gaidelis, V. Jankauskas, R. Maldzius, S. Jursenas, V. Getautis, *Chem. Eur. J.* **2013**, *19*, 15044–15056.
34. M. Sonntag, K. Kreger, D. Hanft, P. Strohriegl, S. Setayesh, D. de Leeuw, *Chem. Mater.* **2005**, *17*, 3031-3039.
35. Q.-X. Tong, S.-L. Lai, M.-Y. Chan, K.-H. Lai, J.-X. Tang, H.-L. Kwong, C.-S. Lee, S.-T. Lee *Chem. Mater.* **2007**, *19,* 5851–5855.
36. V. Mimaite, J. V. Grazulevicius, R. Laurinaviciute, D. Y. Volynyuk, V. Jankauskas and G. Sini, J. Mater. Chem. C, **2015**,**3**, 11660-11674.
37. D. Gudeika, J. V. Grazulevicius, G. Sini, A. Bucinskas, V. Jankauskas, A. Miasojedovas, S. Jursenas, Dyes and Pigments, **2014**, 106, 58.
38. J. Keruckas, R. Lygaitis, J. Simokaitiene, J. V. Grazulevicius, V. Jankauskas, G. Sini, J. Mater. Chem., **2012**, 22, 3015.
39. J. Jensen, K. Wärnmark, *Synthesis* **2001**, *12*, 1873–1877.
40. E. Miyamoto, Y. Yamaguchi, M. Yokoyama, *Electrophotography* **1989**, *28*, 364–370.
41. M. Cordona, L. Ley, *Top. Appl. Phys.* **1978**, *26*, 1.
42. E. Montrimas, V. Gaidelis, A. Pazera, *Lith. J. Phys.* **1966**, *6*, 569.
43. S. M. Vaezi-Nejad, *Int. J. Electron.* **1987**, *62*, 361–384.
44. Y. Archie, C. Chan, C. Juhasz, *Int. J. Electron.* **1987**, *62*, 625–632.
45. K. Wojciechowski, T. Leijtens, S. Siprova, C. Schlueter, M. T. Hörantner, J. T.-W. Wang, C.-Z. Li, A. K.-Y. Jen, T.-L. Lee, H. J. Snaith, *J. Phys. Chem. Lett.*, **2015**, *6*, 2399–2405.